Journal of Physics: Condensed Matter

PAPER

Ab initio study of negative electron affinity from light metals on the oxygen-terminated diamond (1 1 1) surface

To cite this article: Michael C James *et al* 2019 *J. Phys.: Condens. Matter* **31** 295002

IOP Publishing Journal of Physics: Condensed Matter
J. Phys.: Condens. Matter **31** (2019) 295002 (8pp) https://doi.org/10.1088/1361-648X/ab18ef

Ab initio study of negative electron affinity from light metals on the oxygen-terminated diamond (1 1 1) surface

Michael C James[1,2], **Paul W May**[1] **and Neil L Allan**[1]

[1] School of Chemistry, University of Bristol, Cantock's Close, Bristol, BS8 1TS, United Kingdom
[2] HH Wills Physics Laboratory, Bristol Centre for Functional Nanomaterials, University of Bristol, Tyndall Avenue, Bristol, BS8 1TL, United Kingdom

E-mail: michael.james@bristol.ac.uk

Received 25 February 2019, revised 4 April 2019
Accepted for publication 12 April 2019
Published 7 May 2019

Abstract

Recent computational work has shown that light metals adsorbed onto the oxygenated diamond (1 0 0) surface have the potential to give diamond a temperature-stable negative electron affinity (NEA). Here, we use density functional theory to study three of these metals, lithium, magnesium and aluminium, on the (1 1 1) surface. We show that all three of these metals adsorbed onto the ketone O-terminated diamond surface can possess a large NEA and adsorption energies above that of H-termination at monolayer (ML) or sub-ML coverages. Adsorption onto the ether O-terminated surface gives similarly large NEAs but lower adsorption energies. These results are promising for the development of novel NEA surfaces such as those required for thermionic devices.

Keywords: density functional theory, negative electron affinity, diamond, surface

(Some figures may appear in colour only in the online journal)

Introduction

There has been considerable recent interest in obtaining a negative electron affinity (NEA) surface from diamond. An NEA, where the conduction band (CB) minimum is higher in energy than the vacuum energy, allows electrons located in the CB to escape to vacuum with little energy barrier, making NEA diamond an efficient source of electrons (figure 1). For example, electrons can be emitted by heating the diamond to temperatures around 800 °C (thermionic emission) [1], with applications in thermionic energy converters for solar power generation or waste heat scavenging [2–4]. Electrons can be emitted via field emission, for high-power switches, electron sources or flat-panel displays [5, 6]. High secondary electron yields from NEA diamond have also been reported, for potential use in photomultipliers [7–9]. Alongside the NEA, the corresponding high energy of the valence band (VB) allows surface transfer doping from adsorbates [10]. The deposition of a material with a large positive electron affinity onto the diamond surface can induce a 2D hole gas in diamond and has been used to develop diamond-based electronic devices such as capacitors and field effect transistors [11–13].

Hydrogen termination has been the most widely studied NEA surface on diamond, with an electron affinity of −1.3 eV measured experimentally [14, 15]. H-termination is unstable at elevated temperatures ($\gtrsim$700 °C) [16]; this is problematic for thermionic emission applications which require these high temperatures to thermalise electrons into the CB. At these thermionic operating temperatures hydrogen desorbs from the diamond surface to create a bare surface with positive electron affinity. Therefore, work has focused on finding alternatives to H with which to terminate the diamond surface that retain NEA but are also stable at higher temperatures.

A diamond surface with NEA is believed to originate from termination with a more electropositive species than carbon, creating a dipole with positive charge outermost. Prior computational work has predicted an NEA from diamond terminated with group I metals and first-row transition metals (TMs) [17–20]. Experimentally, diamond exhibits an NEA upon deposition of thin layers of various TMs [21–24], or

from termination with Si [25] or Ge [26]. Titanium deposition leads to an enhanced thermal stability over H-termination, and the higher emission temperature doubled the obtainable emission current density [27].

There has been particular focus on obtaining NEA from more complex metal–oxygen–diamond surface terminations. This is particularly desirable since typical metal–oxygen and carbon–oxygen bonds are stronger than metal–carbon bonds [28, 29], increasing the thermal stability of the surface termination. Since the metal is already partially oxidised, there is less propensity for it to react further with oxygen, making these surfaces more air stable. Additionally, the partly ionic character of the metal–oxygen bond can enhance the surface dipole, producing a large NEA. One complication is that before the metal is deposited, the oxygen-terminated diamond surface can take several possible forms, with the two most stable involving the oxygen bonding either to a single carbon atom as a ketone (C=O), or bridging across two carbons as an ether (C–O–C).

The majority of research in this area has focused on the (1 0 0) surface, with experimental and computational studies including lithium [18, 30, 31], magnesium [31, 32], aluminium [33], and various first-row TMs [34]. A computational study by O'Donnell *et al* [31] of metal–oxygen–diamond surfaces involving the group I elements showed that the adsorption energies of lighter metals are larger than those of heavier metals, and even though lighter metals are less electropositive, the NEA values are comparable. In contrast to the (1 0 0) surface, the (1 1 1) surface has been far less studied, even though it is the natural cleavage plane of diamond, a dominant growth surface in CVD diamond, and prevalent in nanodiamonds [35–37]. Experimental work with caesium has shown that the Cs–O–diamond termination is more thermally stable on the (1 1 1) surface, up to 500 °C compared with 400 °C for the (1 0 0) surface [38, 39]. In this paper we consider adsorption of Li, Mg and Al each at 0.25, 0.5 and 1 monolayer (ML) coverages on the ether and ketone O-terminated (1 1 1) diamond surfaces. These three light metals exhibit promising NEA properties on (1 0 0) diamond and we now investigate their properties on the (1 1 1) surface.

Method

Density functional theory (DFT) calculations were performed using the plane-wave CASTEP code [40] on a diamond slab consisting of 14 carbon layers. In all calculations, the diamond slab surfaces were 2 × 2 supercells of the primitive (1 1 1) surface cell, and periodic in two dimensions. Lattice vectors parallel to the surface were both fixed to 5.05 Å, and the angle between them was fixed to 120°. Terminations were applied to both the top and bottom surfaces to prevent any charge imbalance across the slab. A vacuum gap of approximately 20–25 Å separated repeating slabs to ensure no interaction between surfaces. A basis set of plane waves with an energy cut-off of 700 eV, the Perdew–Burke–Ernzerhof (PBE) generalised gradient approximation (GGA) for the exchange-correlation functional [41] and Vanderbilt pseudopotentials [42]

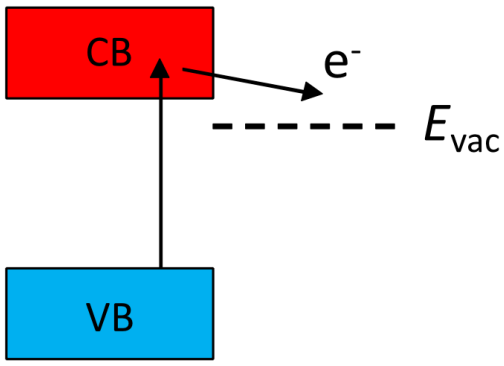

Figure 1. A NEA exists when the minimum energy of the CB lies higher than the vacuum level energy, E_{vac}. This situation allows bulk electrons energized from the VB to the CB to escape into vacuum with virtually no energy barrier.

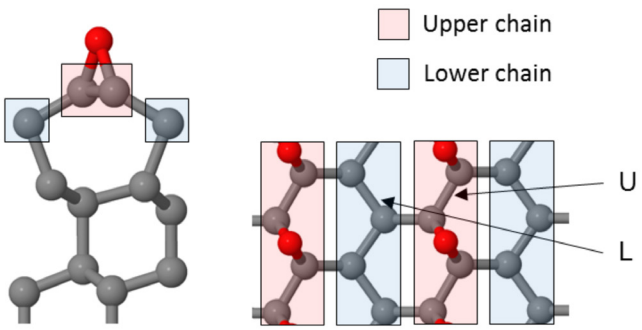

Figure 2. Side and plan view of the half-oxidised O-terminated ether (1 1 1) surface. Adsorption sites are assumed to be 2-coordinate to O atoms with the chosen metal either above the upper (U) or lower (L) Pandey chain.

were used in all calculations. Density-of-states spectra were computed using the OptaDOS code [43] with adaptive broadening and DOS spacing of 0.07 eV. The Brillouin zone was sampled by a 6 × 6 × 1 Monkhorst–Pack *k*-point grid [44] for energy minimisation steps and a 12 × 12 × 1 *k*-point grid for DOS calculations. The validation of these computational parameters has been shown previously [33].

Calculations of ionisation energies, I, were adapted from the method of Fall *et al* [45] in which the energy of the valence band maximum (VBM) of the slab, E_{VBM}, is determined from the addition of the average electrostatic potential of the slab, V_{slab}, to the difference between the VBM position in bulk diamond, $E_{VBM,\,bulk}$, and the average electrostatic potential of bulk diamond, V_{bulk}. This energy is then subtracted from the vacuum energy, E_{vac}, as shown by equation (1).

$$I = E_{vac} - E_{VBM} = E_{vac} - (V_{slab} + E_{VBM,bulk} - V_{bulk}). \quad (1)$$

The electron affinity, χ, is calculated from the subtraction of the band gap of diamond, E_g, from the ionisation energy (equation (2)). The experimental value for bulk diamond is used since the GGA method underestimates the band gap of diamond [19].

$$\chi = I - E_g. \quad (2)$$

The adsorption energy, E_{ads}, was calculated by subtraction from the total energy of slab plus adsorbates, E_{total}, the slab

Table 1. Adsorption energy, E_{ads}, ionisation energy, I, electron affinity, χ, metal–oxygen bond lengths, d(M–O) and the Mulliken charge on the metal ion for metal addition to the half-oxidised ether O-terminated (1 1 1) surface. E_{ads} for the metal-free surface is taken with respect to the bare surface.

Metal	Coverage (ML)	Site (s)	E_{ads} (eV/atom)	I (eV)	χ (eV)	d(M–O) (Å)	M charge (e)
—	0	—	−6.18	7.61	2.14	—	—
Li	0.25	U	−3.05	4.43	−1.04	1.84	0.94
Li	0.25	L	−2.82	4.55	−0.92	1.77	0.96
Mg	0.25	U	−3.03	2.97	−2.50	1.96	1.44
Al	0.25	U	−4.65	5.12	−0.35	1.74	1.19
Al	0.25	L	−5.08	4.79	−0.68	1.74	1.73
Li	0.5	U	−3.52	1.60	−3.87	1.70, 1.86	0.64, 0.96
Li	0.5	U + L	−2.81	2.52	−2.95	1.71, 1.78	0.68, 0.96
Mg	0.5	U	−2.87	5.58	0.11	1.95, 2.04	0.71, 0.69
Mg	0.5	U + L	−3.15	5.40	−0.07	1.92, 1.96	0.70, 0.76
Al	0.5	U + L	−4.76	6.25	0.78	1.84, 1.85	0.74, 0.72

energy with no adsorbate, E_{slab}, and the number, N, of isolated adsorbate atoms of energy, E_{at}. This is divided by the total number of adsorbate atoms to give energy per adsorbate (equation (3)). A negative E_{ads} indicates exothermic adsorption.

$$E_{ads} = (E_{total} - E_{slab} - NE_{at})/N. \quad (3)$$

Surface structures

Initially, the adsorption energy and electron affinity were calculated for the hydrogen-terminated (1 1 1) surface for comparison with subsequent terminations. The H-terminated surface is lowest in energy with no reconstruction, in agreement with experiment [46]. The calculated adsorption energy is −3.79 eV, which is smaller than the value of −4.89 eV obtained by Loh *et al* [47]. The adsorption energy is taken with respect to the energy of an unterminated (1 1 1) surface with (2 × 1) reconstruction, where surface carbons form a zig-zag π-bonded 'Pandey' chain along the surface [48]. The calculated electron affinity of H-termination is −2.2 eV, in good agreement with other computational work [49, 50]. This is larger than the experimental value of −1.3 eV; it is not uncommon for DFT to overestimate the magnitude of the electron affinity of diamond. This difference may be due to approximations inherent to DFT, or because of defective experimental surfaces.

Unlike on the (1 0 0) surface, where ketone and ether oxygen terminations can be present simultaneously, on the (1 1 1) surface the extent of O coverage is believed to affect how O is bonded to diamond; the ketone can form 1 ML coverage, but the maximum ether coverage is 0.5 ML due to the way oxygen bonds with the surface [47]. It has been argued that steric repulsion between oxygen atoms may limit the total surface coverage of oxygen to 0.5 ML for the (1 1 1) surface experimentally [51], but a similar argument for the (1 0 0) surface was strongly disputed by Zheng *et al* [52] and calculations of adsorption energies suggest 1 ML coverage is possible [39, 47].

We define 1 ML of metal addition as one adsorbate per surface unit cell, so four adsorbates comprise 1 ML of the 2 × 2 diamond supercell used in these calculations. For addition to both ether and ketone O-terminated (1 1 1) surfaces, sites for metal addition are chosen that maximise the metal–oxygen (M–O) coordination number. Coverages of 0.25, 0.5 and 1 ML are studied, representing 1, 2 and 4 metal atoms, respectively, added to the diamond surface 2 × 2 supercell.

Metal addition to the ether surface

The ether oxygenated (1 1 1) diamond surface retains the (2 × 1) reconstructed Pandey chain structure observed for the bare surface [47]. Oxygen atoms bridge two C atoms in the upper Pandey chain at 0.5 ML coverage. Figure 2 shows the ether surface with the sites considered for metal addition shown in the plan view.

Table 1 shows results for Li, Mg and Al adsorption at different sites and coverages to the ether O-terminated (1 1 1) surface, and figure 3 shows the sites with the largest calculated NEA. For each metal, one C–O bond from each ether breaks at sub-ML coverages, allowing a M–O bond to form. There is little difference between adsorption energies at 0.25 and 0.5 ML coverage. Al has the largest adsorption energy while Li and Mg have similar, lower energies; only the adsorption energy of Al is larger than that of H-termination. At 1 ML both C–O bonds break and oxygen atoms are incorporated into the metal layer. This is a different result to that in previously reported computational work for Li at 1 ML [53, 54], and possible reasons for this are discussed later.

During energy minimisation, a small amount of atomic rearrangement occurs; after the ether bond breaks oxygen and metal atoms move slightly from their initial positions. For metal atoms at the L site, only Li remains 2-coordinate to O atoms in one Pandey chain, while Mg and Al are instead 2-coordinate to O atoms across two Pandey chains (e.g. Al in figure 3(c)). As the C–O bonds break, adjacent C atoms form a C=C double bond; Mulliken population analysis [55] shows an increase in the C–C bond population from 0.82 before adsorbate addition to ~1.4 after. Bond populations confirm there is no bonding between metal and surface C atoms. Mulliken charges of the metals give an idea of the degree of

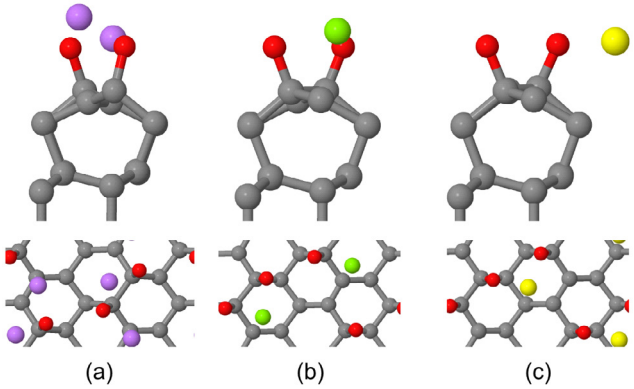

Figure 3. Side and plan views of (a) 0.5 ML Li (purple spheres), (b) 0.25 ML Mg (green sphere), and (c) 0.25 ML Al (yellow sphere) adsorption to the ether O-terminated surface. These are the adsorption sites that gave the largest NEA. Carbon and oxygen are represented as grey and red spheres, respectively.

ionisation of the metals. As shown in table 1, at 0.25 ML coverage values up to 0.96*e*, 1.44*e* and 1.73*e* are observed for Li, Mg and Al, respectively. As expected, on increasing the metal:oxygen ratio each metal atom becomes less positively charged, with the charge on Al changing the most and Li the least. For a given metal smaller M–O bond length and higher metal charge result in a more NEA.

Addition of these metals to the ether surface generally gives NEA, up to −3.87 eV for Li, −2.50 eV for Mg and −0.68 eV for Al. This occurs at 0.5 ML for Li and 0.25 ML for Mg and Al. Mg and Al have a positive electron affinity at 0.5 ML.

Metal addition to the ketone surface

The ketone oxygenated (1 1 1) diamond surface also retains the (2 × 1) reconstruction [47], although the C=O double-bond breaks one of the C–C bonds of the upper Pandey chain, resulting in the elongated hexagonal pattern observable in the plan view (figure 4). In this configuration, O atoms have 1 ML coverage. Adsorbed metals can be 3-coordinate to O and are either located above the upper or the lower Pandey chain.

Table 2 summarises the results for metal addition at various coverages, and figure 5 shows the structures with the largest NEAs for each metal. Adsorption energies all decrease with increasing coverage, which is beneficial experimentally for avoiding island formation of the metal. Li, Mg and Al have adsorption energies up to −5.65 eV, −5.27 eV and −7.31 eV, respectively, for 0.25 ML coverage. Al overall has the largest and Mg the smallest adsorption energies at each site and coverage, which correlates to the M–O bond lengths. Adsorption to the L site is the most favourable at sub-ML coverages except for Mg at 0.5 ML where one Mg atom at the U site and one at the L site is preferred. Compared with adsorption for the H-terminated surface, Li and Al both have a larger adsorption energy at all coverages, while for Mg the adsorption energy is greater at 0.25 and 0.5 ML coverage.

During energy minimisation the metal atoms do not move significantly from their initial positions. Above a certain coverage, the broken C–C dimer of the upper Pandey chain

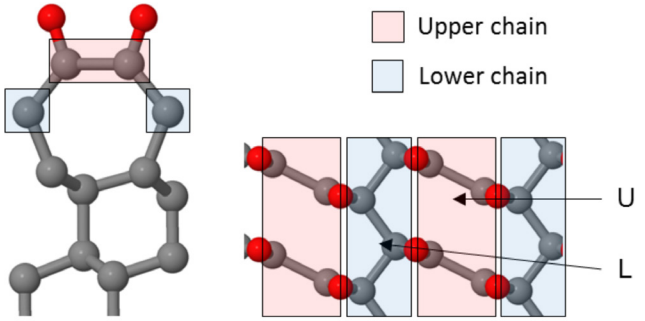

Figure 4. Side and plan view of the fully oxidised O-terminated ketone (1 1 1) surface. Adsorption sites are 3-coordinate to O atoms either above the upper (U) or lower (L) Pandey chain.

reforms. This occurs at 1 ML for Li, 0.5 ML for Mg and 0.25 ML for Al, and is likely to result from the C=O double-bond becoming a C–O single bond. Mulliken bond population analysis shows a decrease in the C–O bond populations with metal addition, from 1.21 for the adsorbate-free surface to minimum values of 1.11, 0.96 and 0.73 for Li, Mg and Al, respectively, at 0.25 ML coverage. With increasing coverage, these values all decrease further, with Li the largest and Al the smallest C–O bond populations. The trend from C=O to C–O parallels the increase in the M–O bond strength. M–O bond populations vary between 0.09–0.49. Al differs from the other metals by consistently showing a positive Al–Al bond population at >0.25 ML coverage, consistent with a metallic Al–Al bond forming.

Negative electron affinities are large for all three metals, with the most negative values −3.74 eV, −3.08 eV and −2.17 eV for Li, Mg and Al, respectively. As with the ether surface, Al has a positive electron affinity in some sites at 0.5 ML coverage, and Mg follows a similar trend in that the electron affinity becomes less negative with increasing coverage. The NEA for Li is again largest at 0.5 ML coverage, unlike Mg and Al. Li can only possess a maximum charge of +1 so it appears for Li that a higher coverage than 0.25 ML is required to maximise the effects of the M–O dipoles. Mulliken charges show each metal becomes highly positively charged at 0.25 ML coverage, up to 0.91*e*, 1.47*e* and 2.13*e* for Li, Mg and Al, respectively. Again, as metal coverage increases, Mulliken charges for each metal becomes less positive, as expected given the reduction in the M:O ratio, and both M–O bond length and metal charge correlate with the electron affinity.

Electronic structure

Partial density-of-states (PDOS) spectra were computed to analyse contributions to the electronic structure from individual atoms or groups of atoms. These were computed for the ketone O-terminated (1 1 1) surface, as it has the most promising NEA properties. Shown in figure 6 is the PDOS spectrum for the adsorbate-free ketone surface. The spectrum has the VBM set to zero, and different groups of atoms are offset for clarity. Bulk carbon atoms are chosen from the centre of the diamond slab and indicate the position of the band gap of bulk

Table 2. Adsorption energy, E_{ads}, ionisation energy, I, electron affinity, χ, metal–oxygen bond lengths, d(M–O), and the Mulliken charge on the metal ion for metal addition to the fully oxidised ketone O-terminated (1 1 1) surface. The U site for Mg at 0.5 ML coverage is not an energy minimum. E_{ads} for the metal-free surface is taken with respect to the bare surface.

Metal	Coverage (ML)	Site(s)	E_{ads} (eV/atom)	I (eV)	χ (eV)	d(M–O) (Å)	M charge (e)
—	0	—	−5.82	8.98	3.51	—	—
Li	0.25	U	−5.49	3.54	−1.93	1.85	0.91
Li	0.25	L	−5.65	4.06	−1.41	1.77	0.91
Mg	0.25	U	−4.98	3.25	−2.22	1.88	1.31
Mg	0.25	L	−5.27	2.39	−3.08	1.81	1.47
Al	0.25	U	−6.76	4.94	−0.53	1.77	1.55
Al	0.25	L	−7.31	3.30	−2.17	1.66	2.13
Li	0.5	U	−4.55	2.58	−2.89	1.77	0.74
Li	0.5	L	−4.82	1.72	−3.75	1.70	0.79
Li	0.5	U + L	−4.70	2.11	−3.36	1.68, 1.76	0.79, 0.74
Mg	0.5	L	−3.95	4.82	−0.65	1.88, 1.89	0.91
Mg	0.5	U + L	−4.23	4.87	−0.60	1.87, 1.95	0.89, 0.87
Al	0.5	U	−6.44	5.46	−0.01	1.80	1.10
Al	0.5	L	−6.57	5.79	0.32	1.74	1.23
Al	0.5	U + L	−6.52	5.57	0.10	1.72,1.79	1.24, 1.12
Li	1	U + L	−3.96	4.36	−1.11	1.70, 1.79	0.58, 0.43
Mg	1	U + L	−2.71	5.23	−0.24	1.84, 2.07	0.52, 0.60
Al	1	U + L	−5.08	5.44	−0.03	1.83, 1.94, 1.94, 2.88	0.91, 0.59, 0.59, 0.19

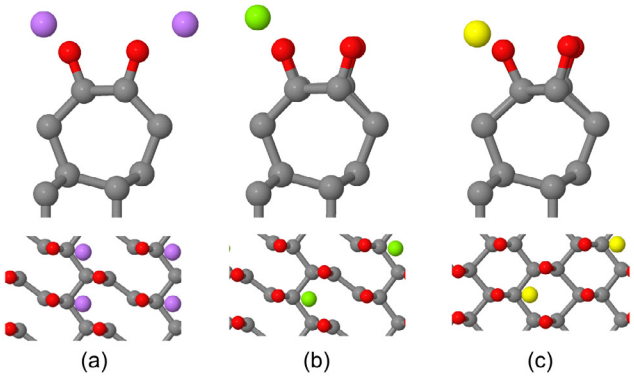

Figure 5. Side and plan views of (a) 0.5 ML Li, (b) 0.25 ML Mg, and (c) 0.25 ML Al adsorption to the ketone O-terminated surface. These are the adsorption sites that gave the largest NEA.

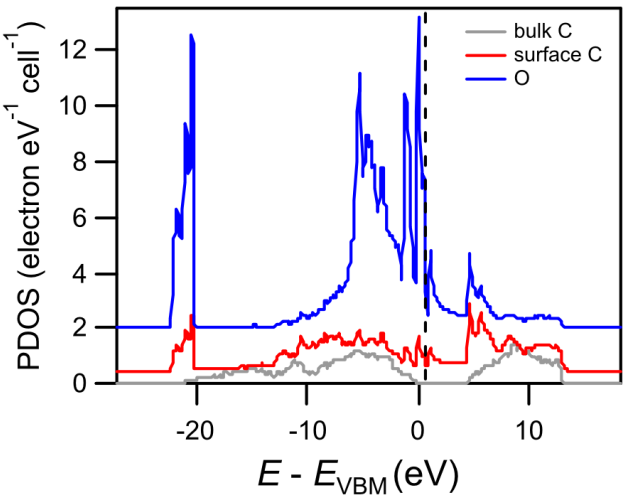

Figure 6. PDOS spectra of the clean ketone oxygenated (111) diamond surface. The dashed vertical line indicates the position of the Fermi level.

diamond. Surface carbon atoms are those in the upper Pandey chain. The peaks for the surface C and the O atoms overlap, indicative of covalent bonding. There are additional peaks for the O atoms in the VB and within the band gap region of the bulk diamond, originating from lone pairs. This is similar to that observed for oxygen on the (1 0 0) surface [50].

Figure 7 shows PDOS spectra for ketone surfaces with adsorbed metals, taken for the lowest energy structures at 0.25 and 0.5 ML coverages given in table 2. 1 ML coverage is not shown as it is associated with lower adsorption energies. In figure 7(a) the DOS for surface C and O both have a peak within the CB region of the bulk diamond. These peaks are lower in energy and within the band gap of bulk diamond in figures 7(b)–(f), and for figures 7(d)–(f) lies just above the Fermi level. The lowering in energy of this peak corresponds to the larger interaction with the metal adsorbate(s), and the change from a C=O bond in figures 7(a)–(c) to a C–O bond in figures 7(d)–(f).

Turning to the metal DOS, Li has little contribution to the DOS except at energies ~4 eV above the VBM at 0.25 ML coverage, moving down in energy to be just above the Fermi level at 0.5 ML coverage. The position of the Li DOS above the Fermi level shows that these 2*s* states are unoccupied and so charge transfer has occurred. The behaviours of the DOS for Mg and Al, meanwhile, are similar to one another, although with different peak shapes. At 0.25 ML coverage, the metal DOS lie just above the Fermi level, while at 0.5 ML coverage these DOS move down in energy to be partly above and partly below the Fermi level. The metal states change from being unoccupied to partially occupied, associated with the smaller positive charge, and with an electron affinity less

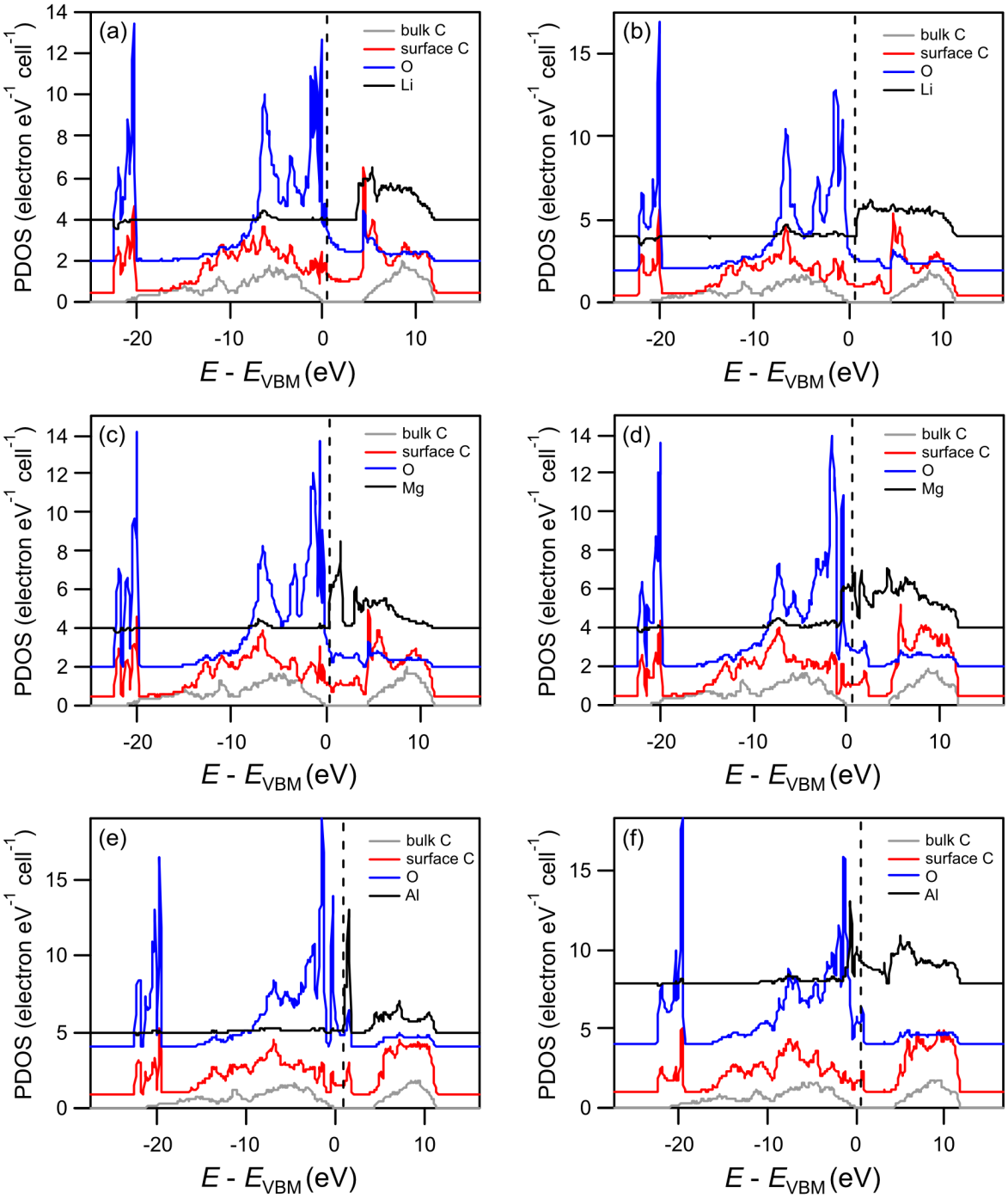

Figure 7. PDOS spectra for (a) and (b) Li, (c) and (d) Mg, and (e) and (f) Al adsorbed onto the ketone surface. The left column (a), (c) and (e) is for 0.25 ML coverage and the right column (b), (d) and (f) is for 0.5 ML coverage. The dashed vertical lines indicate the positions of the Fermi level.

negative at 0.5 ML coverage. Each of the metal DOS display largely ionic behaviour as there is little interaction between the metal and the oxygen states.

Discussion

A comparison of the different oxygen terminations reveals that each metal is more strongly bound to the ketone than to the ether surface. This is not unexpected, as the coordination number to oxygen is greater for metals on the ketone surface. The formation of a strained C=C bond on the upper Pandey chain of the ether surface may also be a contributing factor for the low adsorption energy. Adsorption on the ketone varies more with coverage than on the ether surface, consistent with the larger ionic interaction between the metal and the ketone, which is due to the higher coordination number.

Electron affinities, meanwhile, are broadly similar for the metal-adsorbed ether and ketone surfaces. As the ketone surface has twice the number of O atoms, one might expect that

the ketone electron affinities should be less negative. However, on the ketone surface the metal atoms are more ionised than on the ether surface. This larger surface dipole appears to negate the effect of doubling the number of O atoms, leading to similar values for the electron affinity.

The Li adsorption behaviour reported here for the ether surface differs somewhat from the work of O'Donnell *et al* [53]. In particular, we find no stable surface at 1 ML coverage due to incorporation of O into the metal layer, whereas O'Donnell *et al* report a local minimum where each Li is 2-coordinate to oxygen. It is possible that different computational parameters or convergence criteria contribute to these differences. Alternatively, the larger surface supercell used here gives additional freedom of movement to the atoms. A comparison of the Li-adsorbed ketone surfaces with those in [53] shows the NEAs and adsorption energies are in good agreement and show the same trends.

The adsorption energies for each metal on the ketone (1 1 1) surface are comparable to the (1 0 0) surface for the same coverages [18, 31, 33]. However, the situations which maximise NEA differ; Li and Mg have a slightly larger NEA on (1 0 0) and at higher coverages compared to those on (1 1 1), while Al has larger NEA on (1 1 1) at the same coverage as (1 0 0). Two factors are likely to affect the differences in the adsorption energy and NEA between the (1 0 0) and (1 1 1) surfaces. First, the M–O coordination number is 3 for (1 1 1) and 4 for (1 0 0). The increased coordination number leads to a more positively charged metal adsorbate, affecting the M–O dipole. Second, the coordination geometries of the adsorbates are different. For an adsorbate at the same height above the carbon layer, the M–O bond length on (1 1 1) will be smaller. A comparison shows the M–O bond lengths on the (1 1 1) surface are generally slightly smaller than on the (1 0 0) surface [31, 33].

Conclusions

DFT calculations have been used to study the adsorption of up to 1 ML of Li, Mg and Al onto the ether or ketone oxygen-terminated diamond (1 1 1) surfaces. Adsorption more readily occurs on the ether (1 1 1) surface than the corresponding (1 0 0) surface [33], although with all three metals 1 ML coverage results in the transfer of O atoms from the surface and into the metal layer, breaking all the C–O bonds. For sub-ML coverages large NEAs are predicted.

We find that the metal-adsorbed ketone (1 1 1) surfaces have the largest adsorption energies, which are comparable to those of the corresponding metal-adsorbed (1 0 0) surfaces [31, 33]. Al has the largest adsorption energy, then Li, then Mg, but all are larger than for hydrogen-termination. Adsorption energies decrease with increasing coverage, which is beneficial for avoiding island formation of the metal. Large NEAs are observed at 0.5 ML Li and 0.25 ML Mg and Al coverages, but electron affinities become more positive as coverage increases. Li has the most negative NEA, then Mg, then Al. The results here show the potential for NEA devices using CVD diamond. Li is the most favourable for experimental work that prioritises a large NEA, while Al is preferable for work prioritising high thermal stability, although careful control of coverage is required.

Acknowledgments

This work was carried out using the computational facilities of the Advanced Computing Research Centre, University of Bristol—http://bris.ac.uk/acrc/. Structures were created using DL_VISUALIZE [56] and visualised using Jmol—http://jmol.org/. MCJ acknowledges funding from the Engineering and Physical Sciences Research Council (EPSRC) via the Functional Nanomaterials CDT under grant code EP/L016648/1. Data are available at the University of Bristol data repository at https://doi.org/10.5523/bris.tfp3j1ukgee92bo8pd7w28xlc.

ORCID iDs

Michael C James https://orcid.org/0000-0002-0157-989X

References

[1] Koeck F A M and Nemanich R J 2006 Emission characterization from nitrogen-doped diamond with respect to energy conversion *Diam. Relat. Mater.* **15** 217–20
[2] Koeck F A M and Nemanich R J 2017 Advances in thermionic energy conversion through single-crystal n-type diamond *Frontiers Mech. Eng.* **3** 1–11
[3] Xiao G, Zheng G, Qiu M, Li Q, Li D and Ni M 2017 Thermionic energy conversion for concentrating solar power *Appl. Energy* **208** 1318–42
[4] Tiwari A K 2013 Diamond-based thermo–tunnel devices for hostile environments *PhD Thesis* University of Newcastle
[5] May P W 2000 Diamond thin films: a 21st-century material *Phil. Trans. R. Soc.* A **358** 473–95
[6] Harniman R L, Fox O J L, Janssen W, Drijkoningen S, Haenen K and May P W 2015 Direct observation of electron emission from grain boundaries in CVD diamond by PeakForce-controlled tunnelling atomic force microscopy *Carbon* **94** 386–95
[7] Vaz R, May P W, Fox N A, Harwood C J, Chatterjee V, Smith J A, Horsfield C J, Lapington J S and Osbourne S 2015 Measurement of the secondary electron emission from CVD diamond films using phosphor screen detectors *J. Instrum.* **10** P03004
[8] Lapington J S, Taillandier V, Cann B L, Howorth J and Milnes J 2012 Investigation of the secondary electron emission characteristics of alternative dynode materials for imaging photomultipliers *J. Instrum.* **7** C03018
[9] Lapington J S, Taillandier V, Cann B L, Howorth J and Milnes J 2012 Investigation of the secondary electron emission characteristics of alternative dynode materials for imaging photomultipliers *J. Instrum.* **7** E04002 (erratum)
[10] Strobel P, Riedel M, Ristein J and Ley L 2004 Surface transfer doping of diamond *Diam. Relat. Mater.* **430** 439–41
[11] Pakes C I, Garrido J A and Kawarada H 2014 Diamond surface conductivity: properties, devices, and sensors *MRS Bull.* **39** 542–8
[12] Liu J and Koide Y 2018 An overview of high-*k* oxides on hydrogenated-diamond for metal-oxide-semiconductor capacitors and field-effect transistors *Sensors* **18** 1813
[13] Crawford K G, Qi D, McGlynn J, Ivanov T G, Shah P B, Weil J, Tallaire A, Ganin A Y and Moran D A J 2018 Thermally stable, high performance transfer doping of diamond using transition metal oxides *Sci. Rep.* **8** 3342
[14] Maier F, Ristein J and Ley L 2001 Electron affinity of plasma-hydrogenated and chemically oxidized diamond (1 0 0) surfaces *Phys. Rev.* B **64** 165411

[15] Cui J B, Ristein J and Ley L 1998 Electron affinity of the bare and hydrogen covered single crystal diamond (1 1 1) Surface *Phys. Rev. Lett.* **81** 429–32

[16] Paxton W F, Howell M, Kang W P and Davidson J L 2012 Influence of hydrogen on the thermionic electron emission from nitrogen-incorporated polycrystalline diamond films *J. Vac. Sci. Technol.* B **30** 21202

[17] Nie J L, Xiao H Y and Zu X T 2006 First principles calculations on Na and K-adsorbed diamond (1 0 0) surface *Chem. Phys.* **326** 308–14

[18] O'Donnell K M, Martin T L, Fox N A and Cherns D 2010 *Ab initio* investigation of lithium on the diamond C(1 0 0) surface *Phys. Rev.* B **82** 115303

[19] Tiwari A K, Goss J P, Briddon P R, Wright N G, Horsfall A B and Rayson M J 2012 Electronic and structural properties of diamond (0 0 1) surfaces terminated by selected transition metals *Phys. Rev.* B **86** 155301

[20] Tiwari A K, Goss J P, Briddon P R, Wright N G, Horsfall A B and Rayson M J 2012 Effect of different surface coverages of transition metals on the electronic and structural properties of diamond *Phys. Status Solidi* **209** 1697–702

[21] Baumann P K and Nemanich R J 1998 Characterization of copper–diamond (1 0 0), (1 1 1), and (1 0 0) interfaces: electron affinity and Schottky barrier *Phys. Rev.* B **58** 1643–54

[22] Baumann P K and Nemanich R J 1998 Electron emission from metal–diamond (1 0 0), (1 1 1) and (1 1 0) interfaces *Diam. Relat. Mater.* **7** 612–9

[23] Baumann P K and Nemanich R J 1996 Characterization of cobalt–diamond (1 0 0) interfaces: electron affinity and Schottky barrier *Appl. Surf. Sci.* **104–5** 267–73

[24] Baumann P K and Nemanich R J 1998 Electron affinity and Schottky barrier height of metal–diamond (1 0 0), (1 1 1), and (1 1 0) interfaces *J. Appl. Phys.* **83** 2072

[25] Schenk A K, Tadich A, Sear M J, Qi D, Wee A T S, Stacey A and Pakes C I 2016 The surface electronic structure of silicon terminated (1 0 0) diamond *Nanotechnology* **27** 275201

[26] Sear M J, Schenk A K, Tadich A, Spencer B J, Wright C A, Stacey A and Pakes C I 2017 Germanium terminated (1 0 0) diamond *J. Phys.: Condens. Matter* **29** 145002

[27] Köck F A M, Garguilo J M, Brown B and Nemanich R J 2002 Enhanced low-temperature thermionic field emission from surface-treated N-doped diamond films *Diam. Relat. Mater.* **11** 774–9

[28] Luo Y R 2007 *Comprehensive Handbook of Chemical Bond Energies* (Boca Raton, FL: CRC Press)

[29] Ruscic B, Feller D and Peterson K A 2014 Active thermochemical tables: dissociation energies of several homonuclear first-row diatomics and related thermochemical values *Theor. Chem. Acc.* **133** 1–12

[30] O'Donnell K M, Martin T L, Fox N A and Cherns D 2011 The Li-adsorbed C(1 0 0)-(1 × 1):O diamond surface *Mater. Res. Soc. Symp. Proc.* **1282** mrsf10-1282-a05-04

[31] O'Donnell K M, Martin T L and Allan N L 2015 Light metals on oxygen-terminated diamond (1 0 0): structure and electronic properties *Chem. Mater.* **27** 1306–15

[32] O'Donnell K M, Edmonds M T, Tadich A, Thomsen L, Stacey A, Schenk A, Pakes C I and Ley L 2015 Extremely high negative electron affinity of diamond via magnesium adsorption *Phys. Rev.* B **92** 35303

[33] James M C, Croot A, May P W and Allan N L 2018 Negative electron affinity from aluminium on the diamond (1 0 0) surface: a theoretical study *J. Phys.: Condens. Matter* **30** 235002

[34] Tiwari A K, Goss J P, Briddon P R, Horsfall A B, Wright N G, Jones R and Rayson M J 2014 Unexpected change in the electron affinity of diamond caused by the ultra-thin transition metal oxide films *Europhys. Lett.* **108** 46005

[35] Ristein J 2006 Surface science of diamond: familiar and amazing *Surf. Sci.* **600** 3677–89

[36] Balmer R S *et al* 2009 Chemical vapour deposition synthetic diamond: materials, technology and applications *J. Phys.: Condens. Matter* **21** 364221

[37] Lai L and Barnard A S 2011 Stability of nanodiamond surfaces exposed to N, NH, and NH_2 *J. Phys. Chem.* C **115** 6218–28

[38] Loh K P, Foord J S, Egdell R G and Jackman R B 1997 Tuning the electron affinity of CVD diamond with adsorbed caesium and oxygen layers *Diam. Relat. Mater.* **5** 874–8

[39] Loh K P, Xie X N, Yang S W, Pan J S and Wu P 2002 A spectroscopic study of the negative electron affinity of cesium oxide-coated diamond (1 1 1) and theoretical calculation of the surface density-of-states on oxygenated diamond (1 1 1) *Diam. Relat. Mater.* **11** 1379–84

[40] Clark S J, Segall M D, Pickard C J, Hasnip P J, Probert M I J, Refson K and Payne M C 2005 First principles methods using CASTEP *Z. Kristallogr.* **220** 567–70

[41] Perdew J P, Burke K and Ernzerhof M 1996 Generalized gradient approximation made simple *Phys. Rev. Lett.* **77** 3865–8

[42] Vanderbilt D 1990 Soft self-consistent pseudopotentials in a generalized eigenvalue formalism *Phys. Rev.* B **41** 7892–5

[43] Morris A J, Nicholls R J, Pickard C J and Yates J R 2014 OptaDOS: a tool for obtaining density of states, core-level and optical spectra from electronic structure codes *Comput. Phys. Commun.* **185** 1477–85

[44] Monkhorst H J and Pack J D 1976 Special points for Brillouin-zone integrations *Phys. Rev.* B **13** 5188–92

[45] Fall C J, Binggeli N and Baldereschi A 1999 Deriving accurate work functions from thin-slab calculations *J. Phys.: Condens. Matter* **11** 2689–96

[46] Diederich L, Aebi P, Kuttel O M and Schlapbach L 1999 NEA peak of the differently terminated and oriented diamond surfaces *Surf. Sci.* **424** L314–20

[47] Loh K P, Xie X N, Yang S W and Zheng J C 2002 Oxygen adsorption on (1 1 1)-oriented diamond: a study with ultraviolet photoelectron spectroscopy, temperature-programmed desorption, and periodic density functional theory *J. Phys. Chem.* B **106** 5230–40

[48] Pandey K C 1982 New dimerized-chain model for the reconstruction of the diamond (1 1 1)-(2 × 1) surface *Phys. Rev.* B **25** 4338–41

[49] Rutter M J and Robertson J 1998 *Ab initio* calculation of electron affinities of diamond surfaces *Phys. Rev.* B **57** 9241–5

[50] Sque S J, Jones R and Briddon P R 2006 Structure, electronics, and interaction of hydrogen and oxygen on diamond surfaces *Phys. Rev.* B **73** 1–15

[51] Derry T E, Makau N W and Stampfl C 2010 Oxygen adsorption on the (1 × 1) and (2 × 1) reconstructed C(1 1 1) surfaces: a density functional theory study *J. Phys.: Condens. Matter* **22** 265007

[52] Zheng X M and Smith P V 1992 The stable configurations for oxygen chemisorption on the diamond (1 0 0) and (1 1 1) surfaces *Surf. Sci.* **262** 219–34

[53] O'Donnell K M, Martin T L, Edmonds M T, Tadich A, Thomsen L, Ristein J, Pakes C I, Fox N A and Ley L 2014 Photoelectron emission from lithiated diamond *Phys. Status Solidi* **211** 2209–22

[54] Martin T L 2011 Lithium oxygen termination as a negative electron affinity surface on diamond: a computational and photoemission study *PhD Thesis* University of Bristol

[55] Mulliken R S 1955 Electronic population analysis on LCAO-MO molecular wave functions. I *J. Chem. Phys.* **23** 1833–40

[56] Searle B G 2001 DL visualize *Comput. Phys. Commun.* **137** 25–32